Earth and Planetary Science Letters 501 (2018) 78–89

Contents lists available at ScienceDirect

Earth and Planetary Science Letters

www.elsevier.com/locate/epsl

Context matters – Ar–Ar results from in and around the Manicouagan Impact Structure, Canada: Implications for martian meteorite chronology

Steven J. Jaret [a,b,*], Sidney R. Hemming [b,c], E. Troy Rasbury [a], Lucy M. Thompson [d], Timothy D. Glotch [a], Jahandar Ramezani [e], John G. Spray [d]

[a] Department of Geosciences, Stony Brook University, Stony Brook, NY 11794, USA
[b] Lamont-Doherty Earth Observatory, Palisades, NY 10964, USA
[c] Department of Earth and Environmental Sciences, Columbia University, New York, NY 10027, USA
[d] Planetary and Space Science Centre, University of New Brunswick, Fredericton, New Brunswick E3B 5A3, Canada
[e] Department of Earth Atmospheric and Planetary Sciences, Massachusetts Institute of Technology, Cambridge, MA 02139, USA

ARTICLE INFO

Article history:
Received 21 January 2018
Received in revised form 6 August 2018
Accepted 8 August 2018
Available online xxxx
Editor: F. Moynier

Keywords:
impact cratering
shock metamorphism
argon geochronology
martian meteorites
maskelynite

ABSTRACT

As an analog for interpretations of the ages of martian shergottite meteorites, we have conducted an argon isotopic study of plagioclase feldspars exhibiting varying levels of shock from in and around the Manicouagan impact structure, Canada. Plagioclase from the impact melt sheet at Manicouagan yields an age of 215.40 ± 0.16 Ma, which indicates the time of impact. Plagioclase from a clast within melt-bearing breccias of the melt sheet and a hornfels adjacent to the melt sheet yield ages of 216 ± 3 Ma and 218 ± 7 Ma, respectively, which are interpreted to have been reset by contact metamorphism from the impact melt. Country rocks that were unaffected by the impact gives ~849 Ma ages, consistent with the known Grenvillian target rock history. Maskelynite (amorphous plagioclase, which has been transformed in the solid state) yields an age of 567 ± 6 Ma. This age is geologically meaningless because it is not consistent with the target age, the impact age, or regional metamorphic ages at Manicouagan. Our results show that maskelynite argon ages are not meaningful, and that context is critical for proper interpretation of impact-affected argon ages.

1. Introduction

Determining the timing of impact events and the dating of shocked material is important for studies of extraterrestrial samples. Presently, our collection of samples from beyond Earth are dominated by meteorites, many of which have experienced violent and complex histories involving at least one large impact event. Therefore, it is critical to understand how impacts have altered our ability to date primary events on meteorite parent bodies. This is particularly the case for Mars, where ages of martian meteorites are debated, and where the degree to which impacts affect radioisotopic chronometers is the topic of much debate (Bouvier et al., 2008, 2009; Stephan and Jessberger, 1992; Park et al., 2013). As such, the interpretation of ages obtained from shocked meteorites can be contentious. The goal of this study is to examine $^{40}Ar/^{39}Ar$ ages from a terrestrial impact structure, where both the impact and original target ages of the rocks are known in order to assess the effects of impact.

1.1. Martian chronology and impacts

Our understanding of martian geology would benefit from absolute chronology. Although there have been attempts to obtain absolute ages directly on Mars (Farley et al., 2014), high precision martian geochronology measurements are presently best obtained from martian meteorites in terrestrial laboratories. Current absolute age estimates for martian samples range from ~150 Ma to more than ~4.3 Ga (Bouvier et al., 2009, 2008; Nyquist et al., 2001). K–Ar analyses by the Curiosity rover of the Sheepbed mudstone yields an age of 4.2 ± 0.35 Ga (Farley et al., 2014). The orthopyroxenite martian meteorite ALH84001 has an Rb–Sr crystallization age of ~4 Ga (Lapen et al., 2010; Nyquist et al., 2001). Nakhlites and Chassignites give Rb–Sr and Sm–Nd ages of 1.4 Ga (Korochantseva et al., 2011) and argon ages of between 1416 ± 7 Ma and 1322 ± 10 Ma (Cohen et al., 2017). U–Pb ages from

* Corresponding author at: Department of Geosciences, Stony Brook University, Stony Brook, NY 11794, USA.
E-mail address: steven.jaret@stonybrook.edu (S.J. Jaret).

https://doi.org/10.1016/j.epsl.2018.08.016
0012-821X/

Table 1
Compilation of radiometric ages of martian meteorites. In addition to there being a variety of ages reported depending on chronometer, there are also differences depending upon what phase was measured.

Meteorite	Ar age (Ma)	Phase	Reference	Notes
Los Angeles	165	'plag'	Bogard et al., 2009	'Plagioclase' is used in this publication for all phases of plagioclase-composition regardless of structural state. No detailed description of shock state is given.
	318	whole rock	Bogard et al., 2009	The methods sections says this sample was taken from an impact melt vein, but no description of this material is presented.
	1428	melt pocket	Walton et al., 2007	Spatially resolved laser probe was used to maintain petrographic context
	1290	matrix adjacent to melt	Walton et al., 2007	Spatially resolved laser probe was used to maintain petrographic context
NWA 3171	232	'plag'	Bogard et al., 2009	The methods sections says this sample was taken from an impact melt vein, but no description of this material is presented
NWA 2975	672	'plag'	Bogard et al., 2009	The methods sections says this sample was taken from an impact melt vein, but no description of this material is presented
Dho 019	721	'plag'	Bogard et al., 2009	The methods sections says this sample was taken from an impact melt vein, but no description of this material is presented
	849	whole rock	Bogard et al., 2009	The methods sections says this sample was taken from an impact melt vein, but no description of this material is presented
Dho 019	643 ± 72	maskelynite	Korochantseva et al., 2009	The methods sections says this sample was taken from an impact melt vein, but no description of this material is presented
Dag 476	1000	'plag'	Bogard et al., 2009	reported as a 'total age.' Does not yield a plateau age
	1400	whole rock	Bogard et al., 2009	reported as a 'total age.' Does not yield a plateau age
	1427	matrix	Walton et al., 2007	Spatially resolved laser probe was used to maintain petrographic context
	2324	shock melt	Walton et al., 2007	Spatially resolved laser probe was used to maintain petrographic context
Zagami	∼217	coarse grained 'plag'	Bogard and Park, 2008	plagioclase and maskelynite are used interchangeably. No detailed characterization of the samples measured is given.
	∼2350	fine grained 'plag'	Bogard and Park, 2008	plagioclase and maskelynite are used interchangeably. No detailed characterization of the samples measured is given.
	242	'feldspar'	Bogard and Garison, 1999	no description of shock level is presented. Note: Park et al. (2013) cites an age of 175 attributed to Bogard and Garison (1999), but that age was not found in the original paper.
	592	mixed phase near melt vein	Walton et al., 2007	Spatially resolved laser probe was used to maintain petrographic context. They note ranges for this sample between 443 and 1049 Ma
SaU 005	>850	maskelynite	Korochantseva et al., 2009	
Shergotty	∼370	maskelynite	Korochantseva et al., 2009	
	387, 167 and 195	'feldspar'	Bogard and Garison, 1999	no description of shock level is presented. Note: Park et al. (2013) cites an age of 175 attributed to Bogard and Garison (1999), but that age was not found in the original paper.
	254 ± 10	maskelynite	Bogard et al., 1979	Uses plagioclase and maskelynite interchangeably
NWA 1068	2308 and 4439	melt pocket	Walton et al., 2007	Spatially resolved laser probe was used to maintain petrographic context
ALH 7005	2700	shock melt	Walton et al., 2007	less shocked maskelynite than ALH 7005
ALH 7005	373–>4000	highly shocked plagioclase	Walton et al., 2007	less shocked maskelynite than ALH 7005
ALH 1951	4600	shock melt	Walton et al., 2007	less shocked maskelynite than ALH 7005
ALH 1951	382	maskelynite	Walton et al., 2007	less shocked maskelynite than ALH 7005

zircons within the "Black Beauty" breccia yield ages of 4.4, 1.7, and 1.4 Ga (Agee, 2014). The shergottites, which make up the majority of the martian meteorite collection, yield younger and more varied argon ages, between 150 and 500 Ma (Table 1). Shergottites have experienced moderate shock levels, with the majority of plagioclase converted to maskelynite (Tschermak, 1872; Fritz et al., 2005). Additionally, these samples have discrepancies between chronometers, such as Sm–Nd or Rb–Sr, used for the same samples, which has led to the suggestion that the "young" argon ages date a resetting event, presumably by impact or aqueous processes (Gaffney et al., 2011).

Bouvier et al. (2008, 2009) challenged the notion of "young" ages for the martian shergottites based on Pb isotopes. Using reversed Pb–Pb isochrons of step-wise leached whole rocks, they showed that the common lead-stripped $^{207}Pb/^{206}Pb$ dates representing the radiogenic end-member point to consistently older ages (>4 Ga) for shergottites. They attribute the younger argon ages to resetting due to post-crystallization impact(s).

1.2. Shock resetting of the K–Ar system

Attempts to understand impact-resetting have focused primarily on the K–Ar isotopic system. Of the long-lived chronometers (Rb–Sr, Sm–Nd, U–Pb, K–Ar), the K–Ar system is the easiest to reset during conventional regional and thermal metamorphism (e.g., Bickford and van Schmus, 1979). Shock resetting of the K–Ar system, however, is a complex, disequilibrium process. During impacts, deformation occurs in two fundamentally different ways: isochemical, pressure dominated changes (e.g., formation of high pressure polymorphs and the development of diaplectic glasses), and thermally controlled processes (e.g., impact melting). Coherent impact melt rocks are known to yield ages consistent with the time of impact (Young, 2014) because these rocks crystallized directly from the impact melt just after the impact event. Resetting of the K–Ar system is predominantly understood as a thermal process, and shock-deformed, unmelted material has been thought to be resistant to complete argon resetting because the thermal pulse associated with the shock wave is extremely short. Much of this assumption comes from shock experiments, which show no change in the behavior of the K–Ar system up to shock pressures of 52.5 GPa (Stephan and Jessberger, 1992). However, it is worth noting that typical shock experiments of this scale cannot duplicate the shock pulse durations or heat generated during natural crater forming events on planetary bodies (Fritz et al., 2017).

Numerous radioisotopic isotopic studies have been undertaken on shocked meteorites over the last several decades (Bogard et al., 1987, 1979; Walton et al., 2007; Weirich et al., 2012; Park et al., 2013; Bogard and Garison, 1999), but the many results have been challenging to interpret because meteorites lack the geologic context that could provide independent assessment of their pre-impact formation histories compared to their impact-induced ejection histories. The work presented here aims to test how calculated ages for: a) unshocked target rocks (pre-impact), b) impact melt rocks, and c) shocked rocks (unmelted) from the Manicouagan impact crater compare with one another. Since the target rock ages and the impact age are well known for this crater, this approach should offer valuable insight into the interpretation of Ar–Ar results from maskelynite bearing meteorites.

1.3. Maskelynite and shock state

The term maskelynite, originally described from the martian meteorite Shergotty by Tschermak (1872), defines an amorphous plagioclase phase that has retained its grain boundary and petrographic texture in thin section. Interpretations of shock level and formation mechanisms for maskelynite have been debated for nearly 50 years (El Goresy et al., 2013; Jaret et al., 2015; Stöffler, 1971). Most workers interpret maskelynite to be a solid-state transformation (Jaret et al., 2015; Stöffler, 1971), although El Goresy et al. (2013) have shown that, in some cases, grains that were initially described as maskelynite can show evidence of melting when viewed via high contrast, high resolution electron microscopy.

This issue of whether or not the plagioclase-composition phase has melted is critical to the interpretation of impacted samples. Following Jaret et al. (2015), we use the term maskelynite to indicate a diaplectic feldspar glass and we base our interpretation of formation mechanism on spectroscopy, where grains deformed by solid-state shock exhibit infrared and X-ray anisotropy, whereas glass quenched from a liquid does not show any anisotropy. Frequently, maskelynite is used as an indicator phase for assigning shock level to a meteorite samples (e.g., Stöffler et al., 1991). Generally, the formation of maskelynite is associated with specific pressure conditions (~30 GPa), and most work has focused on the shock level as a function of pressure. The shock state, however, is dependent on multiple factors including temperature, strain rate, composition, and time and can be highly heterogeneous across even small samples (see review by Fritz et al., 2017).

Specific characterization of the grains analyzed in this study are presented in Sections 4.1, 4.2, and 4.3. A key aspect of this study is that we combine detailed assessment of shock level with geochronology. This allows for a more in-depth characterization, and a discussion of the connection between age measured and shock and thermal processes. Unfortunately, for the martian meteorites this typically has not been done. Most studies rely on separate bulk characterization of shock level with 'maskelynite' and 'plagioclase' often being used interchangeably (e.g., Bogard et al., 2009; Park et al., 2013), despite recognition that the shock level within a given sample can vary such that both crystalline plagioclase and amorphous maskelynite sometimes are present in the same section (Turrin et al., 2018). Only recently has petrographic context been maintained during argon analyses, through either laser probe analyses (e.g., Walton et al., 2007) or careful screening and micro-drilling (e.g., Lindsay et al., 2016).

2. Study site and sample descriptions

2.1. Manicouagan impact structure

The Manicouagan impact structure has a ~85 km rim diameter and was formed in the late Triassic predominantly within Canadian Shield Precambrian rocks that experienced profound regional 0.8–1.0 Ga Grenville orogenesis which completely reset the Ar system (DeWolf and Mezger, 1994). The structure has a well-developed, crystalline, impact melt sheet (e.g., O'Connell-Cooper and Spray, 2011) and a well-exposed melt sheet-target rock contact. Over the last decade Manicouagan has been the subject of a focused research program directed at better understanding the impact process and linking the crater as an analogue site with impact structures on other planetary bodies, such as those on the Moon and Mars (Spray et al., 2010). Notably, Manicouagan has been the focus of extensive dating studies. This includes 1) U–Pb ID-TIMS zircon age of 214 ± 1 Ma (Hodych and Dunning, 1992; 2) a U–Pb single-zircon CA-ID-TIMS age of ca. 215.5 Ma (Ramezani et al., 2005)[1]; 3) (U–Th)/He age from impact melt sheet zircons of 213.2 ± 5.4 Ma (Van Soest et al., 2011); and 4) a U–Pb titanite age from the central uplift of 208.9 ± 5.1 Ma (Biren et al., 2014).

2.2. Manicouagan as an analog for extraterrestrial plagioclase dating

Unfortunately, there is no perfect analog on the Earth for comparison to shocked martian meteorites. Earth has a very limited number of impact structures (~200), and even less involving mafic targets suitable for comparison with Mars. The best petrologic analog is shocked basalts from the Lonar Crater, India (e.g., Agarwal et al., 2016). These are fine-grained basalts similar in composition and texture to shergottites and have similar spectroscopic signatures to remote observations of the martian surface (Wright et al., 2011). However, for the purpose of this argon study, Lonar is not ideal. Lonar samples are fine-grained, K-poor, and young, making argon analyses of single grains challenging. Furthermore, while the age of the target rocks at Lonar is known (65 Ma), the impact age is less well-established, either 570 ka (Jourdan et al., 2011) or 52 ka (Sengupta et al., 1997). For our purposes, we need an analog that is easily measurable, with endmember target and impact ages well established, so that differences in measured age between impact melt and maskelynite are unambiguous.

We chose the Manicouagan impact structure for the following reasons. 1) maskelynite at Manicouagan is approximately the same composition as martian maskelynite (An_{54} for Manicouagan, compared to An_{51} for shergottites). 2) Manicouagan is well dated at 215 Ma based on independent U–Pb zircon ages from the melt sheet. This age is significantly different from the Grenville target ages. Even in the case of mixing or partial resetting these two ages are sufficiently far apart for them to be distinguished. Furthermore, the age of Manicouagan is similar to the younger ~100–300 Ma ages reported for martian shergottites.

As with any analog, Manicouagan maskelynite as a proxy for martian maskelynite is imperfect. The Manicouagan rocks are garnet-bearing anorthosite, which is unlike the martian basaltic meteorites. As we discuss in Section 5, this may have affected how the shock wave propagated though the sample. Additionally, it is unclear that the lithologic context of the maskelynite at Manicouagan is the same as for the martian meteorites. At Manicouagan the maskelynite occurs in the central uplift, in association with

[1] Conference abstract without supporting data or error presented.

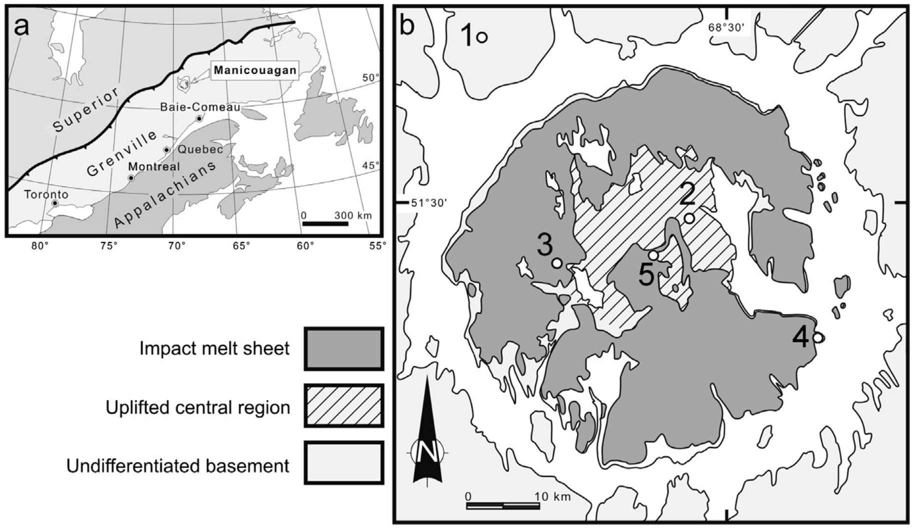

Fig. 1. a) Location of the Manicouagan impact structure, Quebec, Canada; b) Simplified geological map of the Manicouagan impact structure, after Van Soest et al. (2011). Sample locations used in this study: 1 – unshocked anorthositic gneiss, 2 – shocked anorthositic gneiss, 3 – impact melt rock, and 4 – clast-rich melt-bearing breccia, 5 – hornfels (drillcore).

shock veins (Biren and Spray, 2011). We do not know the exact geologic context for the martian maskelynite. A common assumption is that it was formed by shock during the ejection event (Rubin, 2015). In this case, the rocks would have been shocked and immediately ejected into the cold vacuum of space, which is a different post-impact temperature path than at Manicouagan. This assumption, however, is not proven, and the data we have for martian meteorites does not exclusively require maskelynite formation during the ejection event. It is possible (arguably so) that the maskelynite was formed from a prior impact event unrelated to ejection. As we will show in Section 4.2, the maskelynite has a Raman pattern that is similar to that of martian meteorites (Fritz et al., 2005), suggesting they have a similar structural state. We assume – although we cannot be certain – this means they are of similar shock history. It should be noted, however, that Raman spectroscopy can distinguish between crystalline and amorphous material, but this is not a direct correlation to shock level and cannot be used as a direct barometer above the conditions to transform plagioclase to maskelynite (Jaret et al., 2015; Jaret et al., 2018). However, other tests that could potentially distinguish between shock levels within maskelynite have not been systematically applied to martian meteorites and so our use of Raman spectroscopy as a broad screening tool is at present the best available.

Despite the differences between Manicouagan and martian meteorites, given the lack of known context for maskelynite formation on Mars, and well established, significantly different target and impact age, we consider Manicouagan the best analog for our purposes. The important aspect for our study is that we have the ability to measure and compare a variety of impactite samples all from the same event of known time.

2.3. Specific samples measured

Our study uses plagioclase mineral separates from five source lithologies: unshocked country rock, impact melt, shocked country rock, clasts within melt-bearing breccia, and a hornfels from the contact aureole around the melt sheet (Fig. 1). Unshocked samples were collected from Mont Brilliant garnet-bearing meta-anorthosites exposed in the NNW of the structure, where plagioclases are labradorite in composition and 0.25–1 mm in size. Impact melt samples were collected from Observation Lake and are fine-to-medium grained quartz monzodiorite. The maskelynite samples were collected from Mont de Babel and Maskelynite Peak, within the central uplift. They are medium-to-coarse-grained anorthosites (>1 mm), where the plagioclase (labradorite) has been locally converted to maskelynite in association with shock veins (Biren and Spray, 2011).

3. Methods

3.1. Sample preparation

For all samples, we analyzed individual plagioclase (or maskelynite) grains separated from the host rock. Unshocked target rocks were crushed by hand. Maskelynite was either crushed by hand or disaggregated using the SELFRAG® g electronic-pulse disaggregation system at Lamont-Doherty Earth Observatory. Melt-rocks were disaggregated with the SELFRAG®. Xenocrystic grains were obtained by cutting clasts out of the melt-breccia. Melt was then ground off the clasts by hand before they were disaggregated with the SELFRAG® and then handpicked.

For each sample, individual grains were mounted on double-sided tape for micro-Raman analysis to ensure grains grouped together were the same composition and structure. Plagioclase grains from the impact melt rock were small (<1 mm) and in order to obtain radiogenic argon, multiple grains were analyzed together. Additional, doubly-polished thin sections of each sample were prepared for optical petrography (using a standard Olympus petrographic microscope) and micro-Raman spectroscopy.

3.2. Micro-Raman spectroscopy

We collected micro-Raman spectra using a WiTec alpha300R confocal imaging system, in the Center for Planetary Exploration at Stony Brook University. Spectra were collected using a 532 nm Nd YAG laser through a 20X (0.45 NA) objective giving a spot size of 1.41 μm. Each spectrum was acquired with a laser power of 2.25 mW and consisted of 60 acquisitions each with a 1 s integration time. For larger grains (>250 μm) 2 or 3 spectra were acquired per grain.

3.3. Micro-FTIR spectroscopy

We collected micro-FTIR point spectra of single grains in thin section using a Nicolet iN10MX FTIR microscope, in the Center for

Planetary Exploration at Stony Brook University. This instrument is equipped with a liquid nitrogen-cooled HgCdTe array detector capable of acquiring hyperspectral image cubes between 715 and 7000 cm^{-1} (1.4–14 μm) at 25 μm/pixel spatial sampling and a spot size of 100 × 100 μm. To test for preservation of orientation effects, multiple grains were measured with the assumption that the thin section captures a random sampling of grain orientations (Jaret et al., 2015).

3.4. $^{40}Ar/^{39}Ar$ analysis

Feldspar grains with similar position and intensities of the primary Raman peak (514 and 585 Δcm^{-1}) were hand-picked based on micro-Raman spectroscopy (Section 3.2). Grains selected for argon analysis were co-irradiated with Fish Canyon and Fire Clay sanidine monitors for 8 h at the USGS TRIGA reactor in Denver, CO. Interfering isotopes produced by nucleogenic reactions during irradiation were corrected using the production ratios of Dalrymple et al. (1981), specifically:

$^{(39/37)}Ca = 7.11e{-}4$; $^{(38/37)}Ca = 3.29e{-}5$;

$^{(36/37)}Ca = 2.81e{-}4$; $^{(38/39)}K = 1.314e{-}3$;

$^{(40/39)}K = 1.003e{-}3$; and $^{(37/39)}K = 3.32e{-}4$

Argon analyses were performed on a VG5400 at AGES (Argon Geochronology for Earth Sciences) at Lamont Doherty Earth Observatory. Samples were degassed with single-step total fusion using a CO_2 laser, or by step-heating encapsulated samples in Ta tubes with a diode laser. For step-heated samples, multiple grains (between 3 and 6) were loaded for each experiment. In some cases, because of the low Ar abundances, samples were combined from multiple irradiation pits. However, all samples that were combined for step-heating were from the same irradiation level. The released gases were admitted into an automated extraction system for clean-up (300 s with for the single-step samples and for 660 s with the step-heated samples), during which the gases were exposed to Zr–Fe–V metal alloy getters set at 2 amps to strip off reactive gases such as H_2, CO, CO_2, and N_2. The remaining gas was admitted into the VG5400 mass spectrometer where isotopic measurements were collected by peak hopping in static mode using an analogue multiplier. The sensitivity of the system is $\sim 1 \times 10^{-15}$ mol/mv (with 10^{11} A resistor).

We used an internal monitor that is being developed at Lamont, the Fire Clay Tonstein (the Fire Clay Tonstein has a zircon age of 314.614 ± 0.038 Ma, Erin Shea and Jahan Ramezani personal communication). We report the ages calculated using the Fire Clay Tonstein as a monitor because this age (315 Ma) is significantly closer to that of the Manicouagan impact event, and because the date of feldspar from the Manicouagan melt is coincident with the U–Pb date when the Fire Clay zircon age is used to calculate the J-value. J values from all pits analyzed from a single irradiation layer are averaged together for this study. Errors reported for age calculations are 1-sigma. The J values used for age calculations are $1.83220 \times 10^{-3} \pm 1.74360 \times 10^{-6}$ for the melt and maskelynite (irradiation USGS52A; Fire Clay 314.60 ± 0.2 $n/n = 12/14$), $1.81520 \times 10^{-3} \pm 2.89800 \times 10^{-6}$ for the hornfels and clast (USGS72B; Fire Clay 314.98 ± 0.5 $n/n = 5/5$), $1.85280 \times 10^{-3} \pm 1.08460 \times 10^{-6}$ for unshocked 1 (USGS61A; Fire Clay 314.45 ± 0.17 $n/n = 26/26$), and $1.85310 \times 10^{-3} \pm 2.98770 \times 10^{-6}$ for unshocked 2 (USGS62B; Fire Clay 314.40 ± 0.2 $n/n = 15/17$). Two populations of Fish Canyon ages from USGS61A and USGS61B are 28.29 ± 0.05 $n/n = 7/9$ and 28.32 ± 0.03 $n/n = 19/24$, which is older than the accepted value of 28.201 ± 0.046 Ma (Kuiper et al., 2008), although overlapping with the value proposed by Renne et al. (2010). Investigations of intercalibration and the use of different monitor standards are ongoing within this lab and in the community. For the purpose of this paper the ∼1% unresolved difference in the Fish Canyon age is not an impediment to the interpretation.

4. Results

4.1. Petrography

The unshocked sample is a garnet-bearing meta-anorthosite, consisting of coarse-grained (1.5–2 mm) plagioclase (labradorite) with minor amount of subhedral garnets (Figs. 2A, S1A). Weak foliation and layering of the garnets is seen both in hand-sample and in thin section. Additionally, the feldspars have undergone minor weathering with some notable sericitization, particularly along grain boundaries.

The maskelynite sample has a similar texture to the unshocked anorthosite, with the exception that the plagioclase has been converted into an amorphous, optically isotropic glass. The amorphization, however, is heterogeneous, with patches of birefringent plagioclase apparent, particularly adjacent to or between garnets (Figs. 2B, S1B).

The impact melt rock is medium-grained and has a bulk composition of quartz monzodiorite (O'Connell Cooper and Spray, 2011), dominated by quartz and feldspars. Two compositions of feldspars are present, with common k-spar overgrowths on more calcic plagioclase (Figs. 2C, S2C). Compared to the unshocked and maskelynite-bearing samples, the melt-rock is finer-grained, with largest grains measuring only ∼0.5–1.0 mm in length.

The hornfels is a plagioclase-dominated sample consisting of 85–90% plagioclase. This sample is friable in hand-sample, and shows granoblastic feldspars with notable triple junctions (Figs. 2D, S2D) indicative of thermal metamorphism. Minor amounts of amphibole and phyllosilicates are also present.

The clast within the melt sheet breccias was separated from a clast-rich red-matrix melt-rock. In hand-sample, clasts of crystalline anorthosite (similar in texture to the unshocked anorthosite) are typically 1.5–2 cm surrounded by a fine-grained melt-matrix (Figs. 3, S1D). Within each clast, accessory phases (garnet, apatite, zircon) are common and define slight foliation. In thin section, while the clast boundary is intact, internally, the clast has been slightly altered and partially recrystallized. This is particularly prominent towards the edges of clasts in closest contact with the melt-matrix.

4.2. Raman spectroscopy

Raman spectra for all feldspars are shown in Fig. 4. Feldspars from the unshocked anorthosite, the melt rock, and hornfels within the melt-breccias exhibit typical Raman spectra of labradorite: strong peaks at 270, 482, and 505 Δcm^{-1}, and weaker peaks at 464 and 561 Δcm^{-1} (Jaret et al., 2018). The clast feldspars show peaks at similar positions, with notable peaks at 482 and 505 Δcm^{-1}, but overall the peak intensities are diminished compared to the other samples.

The maskelynite-bearing sample shows two distinctly different labradorite-composition phases: i) slightly birefringent labradorite, with peaks at 482 and 582 Δcm^{-1}. These peaks are slightly broader and less intense than in the fully crystalline labradorite, and ii) maskelynite, which is characterized by a broad peak at 482 Δcm^{-1} (Fig. 5).

4.3. Micro-FTIR spectroscopy

Crystalline labradorite (from the unshocked sample) exhibit peaks at 900, 990, and 1100 cm^{-1}. The exact position of these

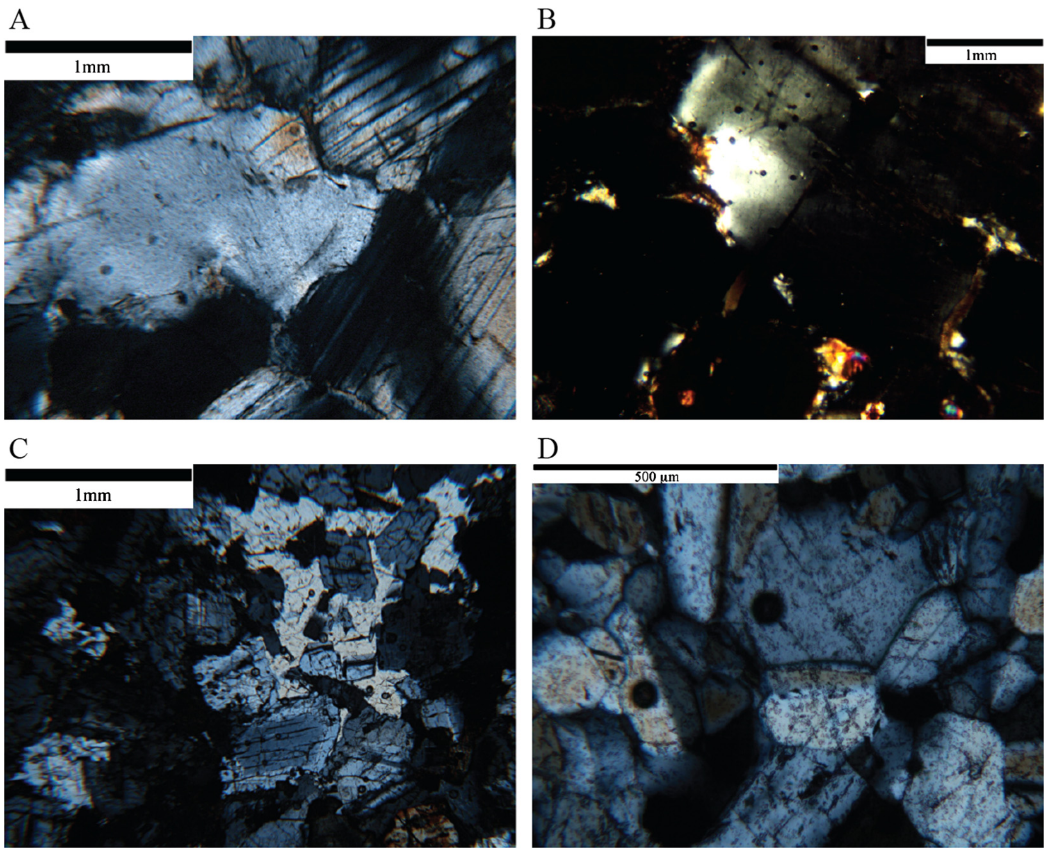

Fig. 2. Cross-polarized photomicrographs of selected samples A) unshocked meta-anorthosite, showing coarse twinned plagioclase with minor amphibole and garnet B) maskelynite, see Fig. 5 for more descriptions. C) Coherent melt-rock, with two compositions of feldspar: plagioclase with kspar rims, and D) hornfels showing slightly smaller grains which have been recrystallized with prominent triple junctions.

peaks is orientation dependent and can vary up to ~40 wavenumbers depending on orientation. Maskelynite samples exhibit only one broad peak centered at 1000 cm^{-1}. This peak also changes with orientation as shown in Fig. S2.

4.4. $^{40}Ar/^{39}Ar$ results

All argon results are reported in Table S1. We analyzed two samples of the unshocked country rocks (Fig. 6). Both samples show somewhat disturbed spectra. One aliquot does yield a plateau age of 849 ± 10 Ma. A second aliquot does not yield a plateau age, but has integrated ages of 840 ± 3 Ma. Both age spectra are consistent with a Grenvillian target rock age, and likely represent cooling from high-grade metamorphism during the Grenville orogeny. Previous Sm–Nd and U–Pb isotopic studies for these rocks yield primary (formation) ages of 1.5 Ga (Thomson et al., 2011) and a major high-pressure, high-temperature metamorphic event at ~1.0 Ga.

Single-step total fusion analyses from plagioclase within the impact melt rock indicate a well-behaved system, with an age probability of 216.60 ± 0.2 Ma (Mean Square Weighted Deviation, MSWD = 1.54). When plotted on an inverse isochron diagram (Fig. 7A), melt samples indicate a slightly elevated initial $^{40}Ar/^{36}Ar$ of 308 ± 7, yielding an age of 215.7 ± 0.9 Ma. Taking the trapped initial $^{40}Ar/^{36}Ar$ into account, the age probability plot for the impact melt is 215.4 ± 0.20 Ma (Fig. 7B).

Step heating analysis of the maskelynite yields an intermediate result between the metamorphic terrane and impact ages, with a poorly defined plateau age of 567 ± 6 Ma (Fig. 8). There is a general correlation between apparent age and $\%^{40}Ar^*$ and the Ca/K, where steps with younger ages have both lower $\%^{40}Ar^*$ and Ca/K. The last step (the final 20% of released ^{39}Ar) has lower $\%^{40}Ar^*$, lower Ca/K, and a younger apparent age. Three single-step total fusion ages of maskelynite yield varied results between 450 and 600 Ma, and are thus consistent with the range of ages from the step heating analyses.

When plotted on an isochron diagram (Fig. 9), the maskelynite samples (individual steps and total fusion data) are clearly scattered, but fall near a 500 Ma reference isochron. The results are entirely contained between modern atmosphere, and endmembers representing the target rocks ($^{40}K/^{40}Ar^*$ for an 800 Ma rock) and the impact ($^{40}K/^{40}Ar^*$ for a 215 Ma rock).

Step-heating experiments of the clasts within the melt-bearing breccias and the hornfels are shown in Fig. S3. Clasts within the melt-breccia yield a plateau age of 216.3 ± 0.8 Ma (Fig. S3A). When plotted on an inverse-isochron diagram (Fig. S4A), this sample has an elevated initial of 306 ± 10 and yields an age of 216 ±3 Ma. The hornfels yields a plateau age of 224.1 ± 1.6 Ma (Fig. S3B). When plotted on an inverse isochron diagram, this sample shows two distinct populations. Using the last 10 steps (black datapoints on Fig. S4B), there is an elevated initial of 320 ± 20 and an age of 218 ± 7 Ma.

5. Discussion

Our measurement of the age of the target rocks at Manicouagan is ~849 Ma, consistent with their location within the Grenville target terrain. This age is slightly younger than the previous K–Ar age estimate of 932 ± 7 Ma (Wolfe, 1971), but given the relatively low closure temperature of the argon system in feldspar, some dispersion in the country rock from the pre-impact geologic history

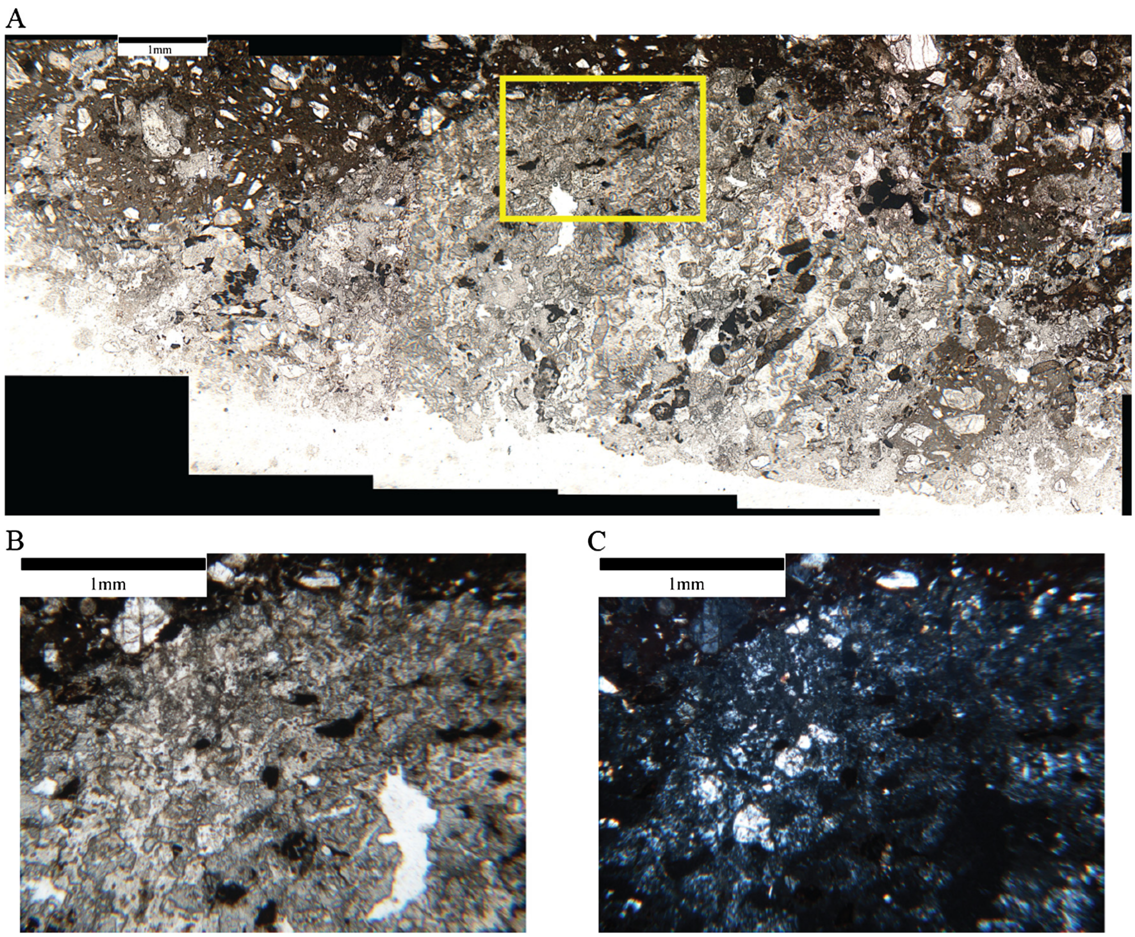

Fig. 3. Thin section photomicrographs of clasts within the melt-matrix breccia. A is a plane-polarized mosaic. B and C are plane- and cross-polarized images taken from the area in A outlined in yellow. The clast is partially recrystallized with alteration minerals more prominent towards the edge of the clast.

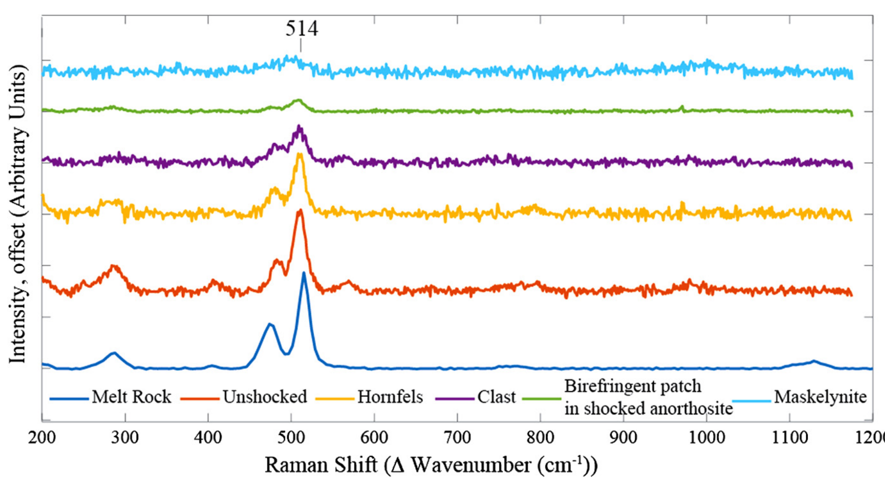

Fig. 4. Raman spectra of phases analyzed for argon. The unshocked, melt-rock, and hornfels show strong peaks at 207, 482, and 507 Δcm^{-1} consistent with crystalline feldspars. The clast within the melt shows weak peaks in positions characteristic of feldspars. The lower intensities of peaks is consistent with partially amorphous or fine-grained material. The maskelynite-bearing sample contains 2 phases (see Fig. 5): slightly birefringent patches which exhibit weak feldspar peaks at 482 and 507 Δcm^{-1}, and optically isotropic regions which show only a broad peak at 482 Δcm^{-1}.

is to be expected. In fact, ages of the Grenville are known to vary laterally across the orogen.

We interpret the time of impact to be 215.4 ± 0.20 Ma as indicated by plagioclase separated from the impact melt. This age is within error of previous estimates of the Manicouagan impact, including the high-resolution ID-TIMS age of 215.5 Ma from zircons within the same sample we measured (Ramezani et al., 2005).

The argon ages of the clast within the melt and the hornfels appear to be essentially reset by the impact event (Fig. S4). The hornfels displays some scatter and there are two populations when plotted on an inverse isochron diagram but calculating the age using the last 10 steps yields an age within error of the impact age. This is consistent with textures (Fig. 3D and Fig. 4), which indicate partial recrystallization and/or metasomatism.

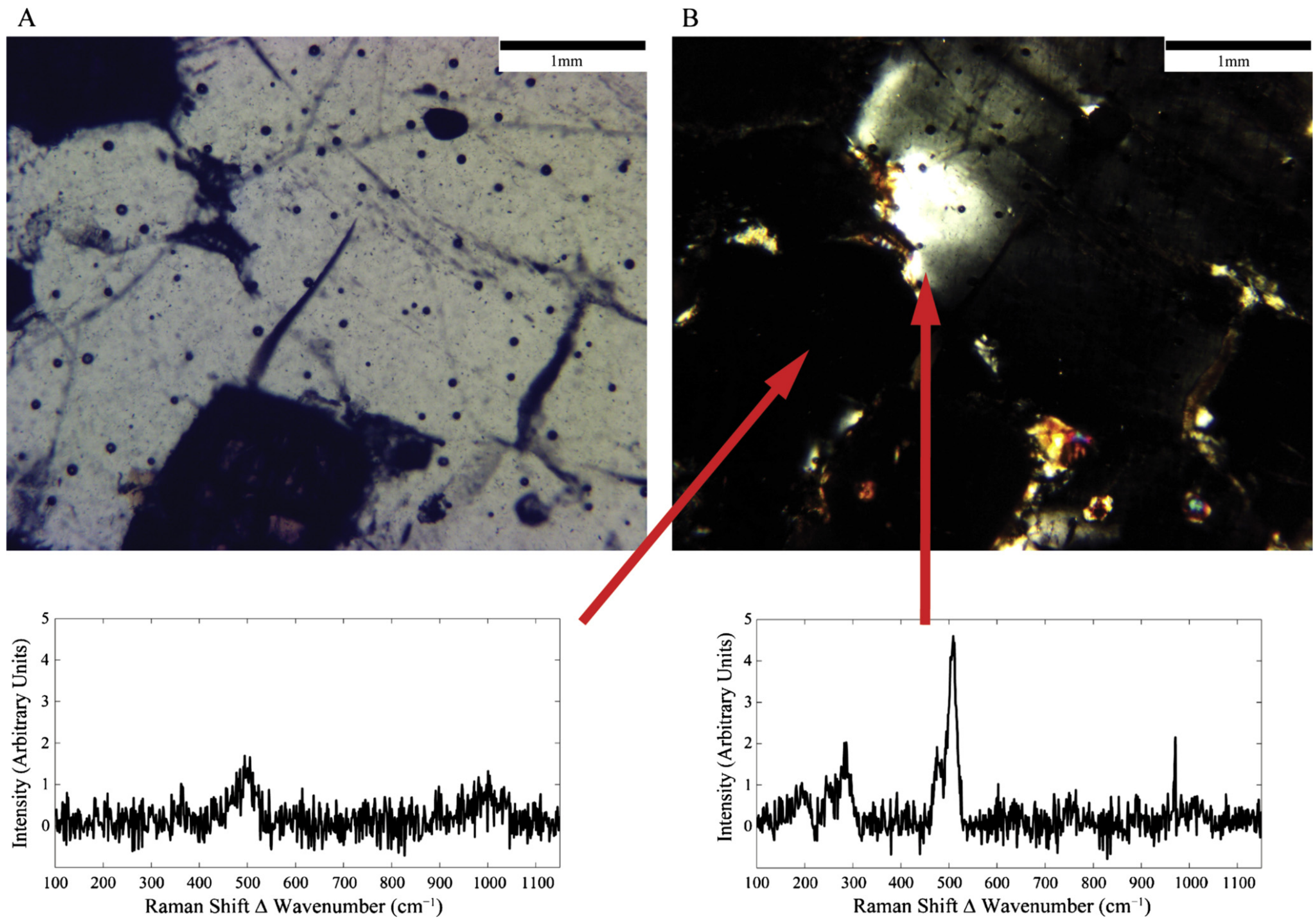

Fig. 5. Photomicrographs (plane-polarized, A, and cross-polarized, B) and micro-Raman spectra of the maskelynite showing the heterogeneous distribution of shock in this sample. Remnant crystalline plagioclase occurs, particularly around and adjacent to garnets.

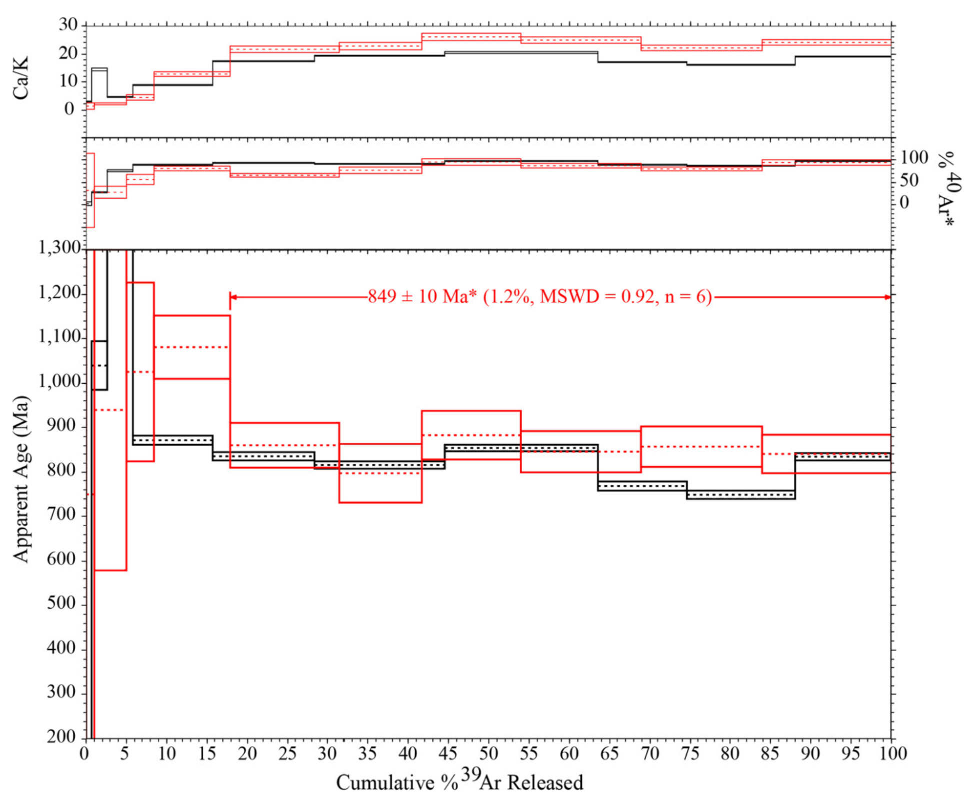

Fig. 6. Ca/K, $\%^{40}Ar^*$, and age spectra of the unshocked anorthosite target rocks. There is some scatter between the two samples, but both yield Grenvillian ages of ∼849 Ma.

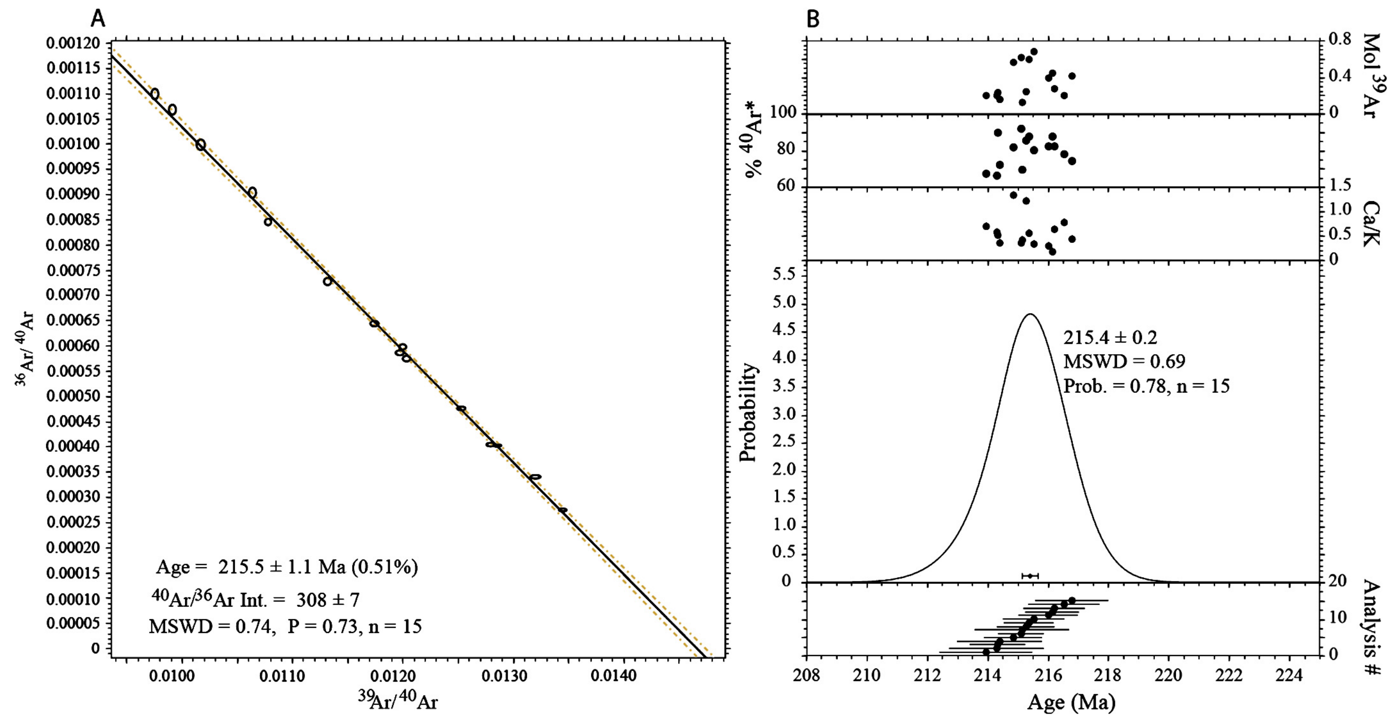

Fig. 7. Argon results for impact melt. A) Inverse isochron from plagioclase in the impact melt (same analyses as plotted in B). The isochron shows a wide range of %radiogenic ^{40}Ar indicates a slightly elevated initial ^{40}Ar/^{36}Ar of 308 ± 7, and an age of 215.5 ± 1.1 Ma. B) Age probability histogram for plagioclase within the impact melt rocks. The age is calculated using the initial ^{36}Ar/^{40}Ar from the isochron in figure A and is 215.4 ± 0.2 Ma.

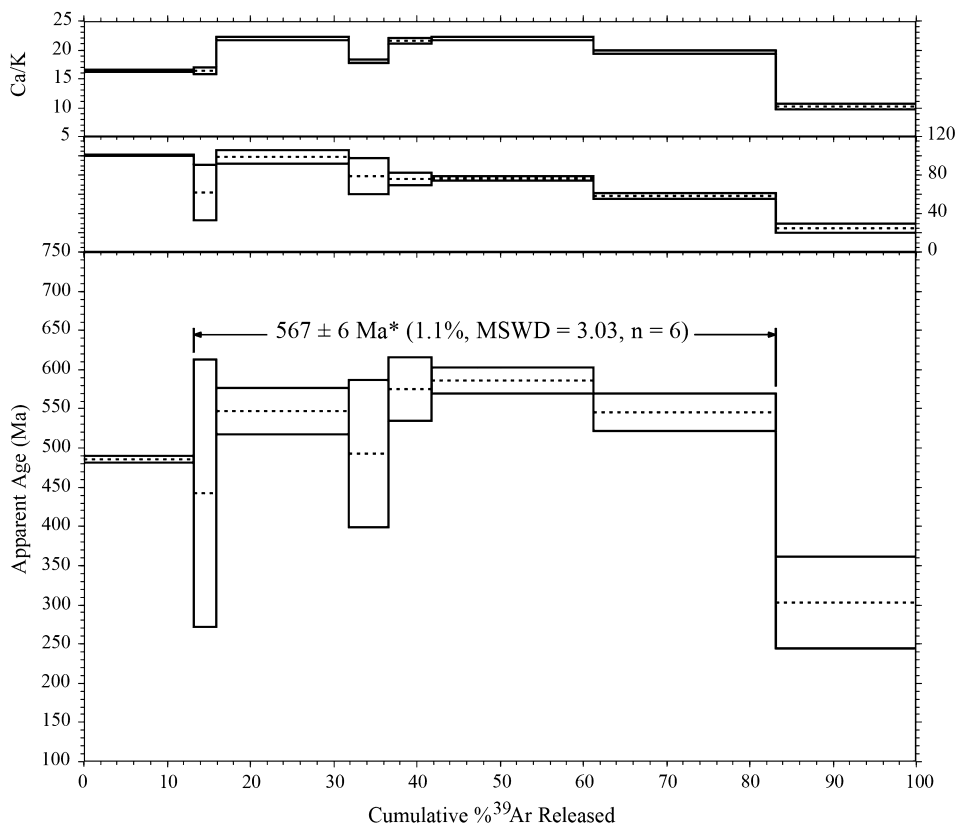

Fig. 8. Ca/K, %^{40}Ar*, and age spectra of the maskelynite. The age spectra shows some scatter, but does define a plateau (as defined by >67% of ^{39}Ar released). The calculated plateau age is 567 ± 6 Ma. There is a slight correlation between Ca/K, %^{40}Ar*, and age particularly in the last step, which shows low Ca/K, low %^{40}Ar*, and younger age. This age is not consistent with target age, impact age nor any metamorphic ages previously reported near Manicouagan.

Apparent ages calculated from our maskelynite samples do not match either the impact age or the target age, but instead are intermediate and without geological significance (Fig. 9). Manicouagan maskelynite samples do not show correlation between subgrain domain and apparent age, but instead appear to have partially lost argon relatively uniformly across all domains. This is

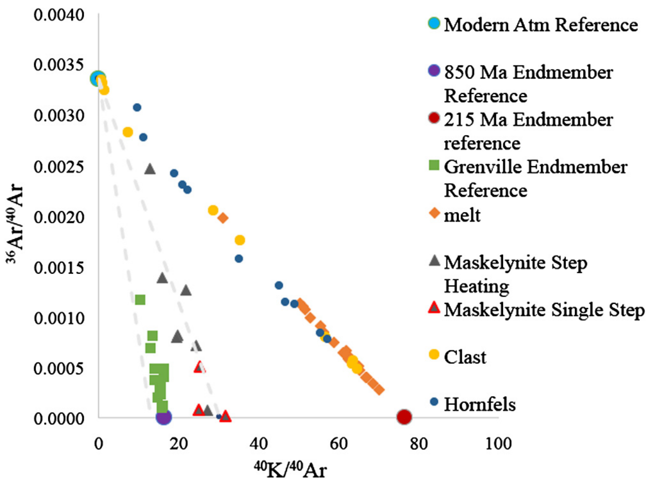

Fig. 9. $^{40}K/^{40}Ar$ vs $^{36}Ar/^{40}Ar$ isotope correlation diagram. Endmembers (circles) include modern atmosphere (blue), $^{40}K/^{40}Ar$ of Grenville target rocks, and $^{40}K/^{40}Ar$ of the time of impact (215 Ma). Reference isochrons at 500 Ma and 100 Ma are shown in grey. Both the impact melt samples (orange diamonds) and the unshocked target rocks (green squares, not including the first 3 heating steps where there appears to be some excess $^{40}Ar^*$). The maskelynite data (triangles) generally correspond with the 500 Ma reference isochron and appears to record partial degassing of the Grenville target at the time of impact. If it were not affected, it would plot with the unshocked Grenville data. If it were completely reset, it would plot with the feldspars from the melt rock. (For interpretation of the colors in the figure(s), the reader is referred to the web version of this article.)

likely related to the structural state of the maskelynite and the argon distribution within the glass. Given the differences in structural state between maskelynite and fused glass (Jaret et al., 2015), future studies may benefit from diffusion measurements and modeling of the behavior of argon in shock-produced maskelynite.

The primary implication of the maskelynite data presented is that it would not be possible to determine the age of the target rock or the impact event from these measurements. The results are best interpreted as the maskelynite has undergone some argon loss during shock, but in a manner that is fundamentally different from thermal metamorphic resetting. While the maskelynite “plateau” is messy, the scatter seen here is of the same order of magnitude that is reported for “plateau” ages of martian meteorites (e.g., Park et al., 2013). Therefore, we suggest that presence or absence of a plateau age is not enough to ensure the age calculated is meaningful.

Individual single-step total fusion ages of maskelynite give a range of ages spanning 400 Ma and 600 Ma. Wolfe (1971) measured similar scatter but interpreted it as a mixing of the end-member target and impact ages. As shown from the $^{40}K/^{40}Ar$ vs. $^{36}Ar/^{40}Ar$ isotope correlation diagram (Fig. 9), the maskelynite data lie entirely within the triangle formed between the target and impact endmembers and modern atmospheric argon. As seen with the age release spectrum (Fig. 8), the maskelynite does not show a systematic increase in age with heating steps that would be associated with partial resetting as a result of metamorphism. In other words, from the maskelynite data alone, it would not be possible to determine that these samples were disturbed at ca. 215 Ma.

The argon result showing partial resetting within the maskelynite is consistent with the spectroscopy results that show that these grains formed via solid-state deformation rather than as melt products. Although the sample is amorphous, the peak position of the Si–O stretching vibration near 1000 cm^{-1} changes slightly with orientation, suggesting this grain transformed without homogenization or melting (i.e., it is a diaplectic glass formed by shock). This is supported by the petrographic textural observations of these rocks in thin section, which show no flow or other indications of melting or mobilization.

One complication in our sampling is the level of shock heterogeneity seen in the maskelynite-bearing sample (Fig. 6). While most of the plagioclase in this sample has been converted to maskelynite, remnant plagioclase regions occur, particularly in and adjacent to garnets. The textures suggest that the garnets are either absorbing or deflecting the shock wave, causing localized heterogeneities in pressure. Practically, choosing loose grains for argon analysis was difficult because once crushed, the amorphous and crystalline plagioclase grains had lost their context and were nearly indistinguishable under a reflected light microscope. To ensure all grains were fully amorphous, we conducted micro-Raman spectroscopy on individual loose grains after picking prior to packaging for irradiation.

There does not seem to be a correlation between the degree of shock-induced structural damage and argon resetting. Maskelynite, the most crystallographically transformed, is partially degassed, but both the hornfels and clasts within the melt-breccia show near complete resetting of argon. Raman spectra (and petrography) of these samples indicate they are still crystalline and have not been transformed to glass. Yet, they are degassed by the impact. Given their direct contact with the melt, this suggests that during impacts, resetting is controlled by heat to a greater degree than by shock level. The crystallinity of the samples (i.e., whether or not it has been transformed to an amorphous material) does not does serve as a predictor of whether or not the sample will be completely reset by the impact. This is similar to He resetting in zircons from within the melt-breccias at the Mistastin impact structure (Young, 2014), but has yet to be shown with the Ar system which has a slightly higher closure temperature than He. This is likely due to the large volume of melt at Manicouagan, which took longer to cool than at smaller impacts like Mistastin.

In the last decade, there has been growing interest in the interpretation of the argon ages of martian meteorites (e.g., Park et al., 2013; Walton et al., 2014), and it has been suggested that $^{40}Ar/^{39}Ar$ ages are not reliable crystallization ages, but reflect the timing of some post-impact resetting. This observation is similar to interpretations made from nahklites (Casatta et al., 2010), and the basaltic achondrite Bunburra Rockhole (Jourdan et al., 2014). It has also been predicted from diffusion models, that indicate plagioclase-composition glass is resistant to resetting by the thermal pulse of the impact, but can be affected by prolonged mid-temperature events such as conductive heating from a melt sheet and post-impact heating in a warm breccia-lens. Our results from Manicouagan demonstrate that while impact-melt rocks are reliable material for dating the impact event, maskelynite is not. Importantly, maskelynite from Manicouagan yields an “age” that corresponds to neither target age nor impact age. If this holds for maskelynite of similar impact conditions then there is reason to suspect maskelynite from martian meteorites could be subject to similar partial resetting. This could be a possible explanation for why some maskelynite grains from within the same shergottites yield ages that differ from each other by as much as 100 Ma, and why the $^{40}Ar/^{39}Ar$ ages of the maskelynite grains do not match those of other chronometers applied to the same meteorites.

These results differ from what has been reported before based on shock experiments, which showed plagioclase to be highly resistant to shock resetting of the Ar isotopic system (Stephan and Jessberger, 1992). The most likely explanation for this discrepancy is that shock experiments are predominately focused on reproducing shock pressures and do not adequately simulate the associated thermal pulse (or pulse duration) of a natural impact. Alternatively, the lack of resetting in shock experiments could be due to differences in timescales of shock experiments and natural shock events. Shock experiments have typical pulse durations of <1 μs, whereas natural impacts have typical pulse durations of 1 s (Fritz et al., 2017). Because the resetting of argon is fundamentally diffusion-based, it is likely that the higher peak temperatures and longer pulse durations associated with natural impacts play a key role in resetting the argon system. While they did not see differences in ages between shocked and unshocked samples in their experiments, Stephan and Jessberger (1992) did see changes in the diffusion rates, and have suggested that this could lead to partial resetting in naturally shocked samples.

6. Conclusions

$^{40}Ar/^{39}Ar$ analysis of plagioclase from the Manicouagan impact melt rock yield an age of 215.4 ± 0.2 Ma. Feldspars in contact with the melt (both as clasts within melt-bearing breccias and in hornfels rocks adjacent to the melt sheet) appear to be completely or near completely reset by thermal metamorphism due to proximity to the melt sheet. Maskelynite, however, yields erroneous "apparent ages" reflecting mixing or partial resetting.

Based on our results from Manicouagan, it appears that maskelynite is not a reliable phase for $^{40}Ar/^{39}Ar$ chronology. The calculated ages obtained from maskelynite do not reflect the timing of any known geologic event at or near Manicouagan. This suggests that $^{40}Ar/^{39}Ar$ ages from maskelynite in martian samples also are not likely to be a real measure of geologic activity on Mars. Instead, these ages could serve as minimum ages for the crystallization of these rock and maximum ages for the time of impact shocking. Argon ages for shergottites span a large range from ∼500 Ma to ∼100 Ma (Korochantseva et al., 2009; Nyquist et al., 2001). Some of this scatter appears to be phase dependent, where maskelynite ages tending to yield older (∼400–500 Ma) ages (Korochantseva et al., 2009). This would indicate that the impact age must be no greater than 100 Ma, and this age reflects partial resetting rather than either an impact or a crystallization age.

Acknowledgements

The Manicouagan Impact Research Program is supported by grants to JGS from NSERC, the Canadian Space Agency FAST program, and the Canada Research Chairs program. This work was supported by a NASA Earth and Space Science Fellowship (NNX13AO57H) to SJJ (2013–2016). We thank (Merry) Yue Cai and Tanzhuo Liu for assistance with argon measurements. Francis (Andy) Winslow provided samples which were collected on a Shoemaker grant for field work. The authors also thank Fred Jourdan and Marc Biren for thoughtful and thorough reviews.

Appendix A. Supplementary material

Supplementary material related to this article can be found online at https://doi.org/10.1016/j.epsl.2018.08.016.

References

Agarwal, A., Kontny, A., Srivastava, D.C., Greiling, R.O., 2016. Shock pressure estimates in target basalts of a pristine crater; a case study in the Lonar Crater, India. Bull. Geol. Soc. Am. 128, 19–28.

Agee, C., 2014. Black beauty: a unique 4.4 Ga, water-rich meteorite from Mars. Elements, 168.

Bickford, M.E., Van Schmus, W.R., 1979. Geochronology and radiogenic isotope research. Rev. Geophys. Space Phys. 17, 824–839.

Biren, M.B., van Soest, M., Wartho, J.-A., Spray, J.G., 2014. Dating the cooling of exhumed central uplifts of impact structures by the (U–Th)/He method: a case study at Manicouagan. Chem. Geol. 377, 56–71. https://doi.org/10.1016/j.chemgeo.2014.03.013.

Biren, M.B., Spray, J.G., 2011. Shock veins in the central uplift of the Manicouagan impact structure: context and genesis. Earth Planet. Sci. Lett. 303.

Bogard, D., Horz, F., Johnson, P., 1987. Shock effects and argon loss in samples of the Leedey l6 chondrite experimentally shocked to 29–70 GA pressures. Geochim. Cosmochim. Acta 51, 2035–2204.

Bogard, D.D., Garrison, D.H., 1999. Argon-39–Argon-40 "ages" and trapped argon in martian shergotites, Chassigny, and Alan Hills 84001. Meteorit. Planet. Sci. 34, 451–473.

Bogard, D.D., Husain, L., Nyquist, L.E., 1979. ^{40}Ar–^{39}Ar age of the Shergotty achondrite and implications for its post-shock thermal history. Geochim. Cosmochim. Acta 43, 1047–1055.

Bogard, D.D., Park, J., 2008. ^{39}Ar–^{40}Ar dating of the Zagami Martian shergottite and implications for magma origin of excess ^{40}Ar. Meteorit. Planet. Sci. 43, 1113–1126.

Bogard, D.D., Park, J., Garrison, D., 2009. ^{39}Ar–^{40}Ar "ages" and origin of excess ^{40}Ar in Martian meteorites. Meteorit. Planet. Sci. 44, 905–923.

Bouvier, A., Blichert-Toft, J., Albarède, F., 2009. Martian meteorite chronology and the evolution of the interior of Mars. Earth Planet. Sci. Lett. 280, 285–295. https://doi.org/10.1016/j.epsl.2009.01.042.

Bouvier, A., Blichert-Toft, J., Vervoort, J.D., Gillet, P., Albarède, F., 2008. The case for old basaltic shergottites. Earth Planet. Sci. Lett. 266, 105–124. https://doi.org/10.1016/j.epsl.2007.11.006.

Cassata, W.S., Shuster, D.L., Renne, P.R., Weiss, B.P., 2010. Evidence for shock heating and constraints on Martian surface temperatures revealed by $^{40}Ar/^{39}Ar$ thermochronometry of Martian meteorites. Geochim. Cosmochim. Acta 74, 6900–6920.

Cohen, B.E., Mark, D.F., Cassata, W.S., Lee, M.R., Tomkinson, T., Smith, C.L., 2017. Taking the pulse of Mars via dating of a plum-fed volcano. Nat. Commun. 8, 640.

Dalrymple, G.B., Alexander, E.C., Lanphere, M.A., Kraker, G.P., 1981. Irradiation of samples for $^{40}Ar/^{39}Ar$ dating using the geological survey TRIGA reactor. U. S. Geol. Surv. Prof. Pap. 1176, 55.

DeWolf, C.P., Mezger, K., 1994. Lead isotopic analyses of leached feldspar: constraints on the early crustal history of the Grenvile Orogen. Geochim. Cosmochim. Acta 58, 5537–5550.

El Goresy, A., Gillet, P., Miyahara, M., Ohtani, E., Ozawa, S., Beck, P., Montagnac, G., 2013. Shock-induced deformation of Shergottites: shock-pressures and perturbations of magmatic ages on Mars. Geochim. Cosmochim. Acta 101, 233–262. https://doi.org/10.1016/j.gca.2012.10.002.

Farley, K.A., Malespin, C., Mahaffy, P., Grotzinger, J.P., Vasconcelos, P.M., Milliken, R.E., Malin, M., Edgett, K.S., Pavlov, A.A., Hurowitz, J.A., Grant, J.A., Miller, H.B., Arvidson, R., Beegle, L., Calef, F., Conrad, P.G., Dietrich, W.E., Eigenbrode, J., Gellert, R., Gupta, S., Hamilton, V., Hassler, D.M., Lewis, K.W., McLennan, S.M., Ming, D., Navarro-González, R., Schwenzer, S.P., Steele, A., Stolper, E.M., Sumner, D.Y., Vaniman, D., Vasavada, A., Williford, K., Wimmer-Schweingruber, R.F., Blake, D.F., Bristow, T., DesMarais, D., Edwards, L., Haberle, R., Hoehler, T., Hollingsworth, J., Kahre, M., Keely, L., McKay, C., Wilhelm, M.B., Bleacher, L., Brinckerhoff, W., Choi, D., Dworkin, J.P., Floyd, M., Freissinet, C., Garvin, J., Glavin, D., Harpold, D., Martin, D.K., McAdam, A., Raaen, E., Smith, M.D., Stern, J., Tan, F., Trainer, M., Meyer, M., Posner, A., Voytek, M., Anderson, R.C.R.B., Aubrey, A., Behar, A., Blaney, D., Brinza, D., Christensen, L., Crisp, J.A., DeFlores, L., Feldman, J., Feldman, S., Flesch, G., Jun, I., Keymeulen, D., Maki, J., Mischna, M., Morookian, J.M., Parker, T., Pavri, B., Schoppers, M., Sengstacken, A., Simmonds, J.J., Spanovich, N., Juarez, M.D.L.T., Webster, C.R., Yen, A., Archer, P.D., Cucinotta, F., Jones, J.H., Morris, R.V., Niles, P., Rampe, E., Nolan, T., Fisk, M., Radziemski, L., Barraclough, B., Bender, S., Berman, D., Dobrea, E.N., Tokar, R., Williams, R.M.E., Yingst, A., Leshin, L., Cleghorn, T., Huntress, W., Manhès, G., Hudgins, J., Olson, T., Stewart, N., Sarrazin, P., Vicenzi, E., Wilson, S.A., Bullock, M., Ehresmann, B., Peterson, J., Rafkin, S., Zeitlin, C., Fedosov, F., Golovin, D., Karpushkina, N., Kozyrev, A., Litvak, M., Malakhov, A., Mitrofanov, I., Mokrousov, M., Nikiforov, S., Prokhorov, V., Sanin, A., Tretyakov, V., Varenikov, A., Vostrukhin, A., Kuzmin, R., Clark, B., Wolff, M., Botta, O., Drake, D., Bean, K., Lemmon, M., Anderson, R.C.R.B, Herkenhoff, K., Lee, E.M., Sucharski, R., Hernández, M.Á.D.P., Ávalos, J.J.B., Ramos, M., Kim, M.-H., Plante, I., Muller, J.-P., Ewing, R., Boynton, W., Downs, R., Fitzgibbon, M., Harshman, K., Morrison, S., Kortmann, O., Palucis, M., Williams, A., Lugmair, G., Wilson, M.A., Rubin, D., Jakosky, B., Balic-Zunic, T., Frydenvang, J., Jensen, J.K., Kinch, K., Koefoed, A., Madsen, M.B., Stipp, S.L.S., Boyd, N., Campbell, J.L., Perrett, G., Pradler, I., VanBommel, S., Jacob, S., Owen, T., Rowland, S., Savijärvi, H., Boehm, E., Böttcher, S., Burmeister, S., Guo, J., Köhler, J., García, C.M., Mueller-Mellin, R., Bridges, J.C., McConnochie, T., Benna, M., Franz, H., Bower, H., Brunner, A., Blau, H., Boucher, T., Carmosino, M., Atreya, S., Elliott, H., Halleaux, D., Rennó, N., Wong, M., Pepin, R., Elliott, B., Spray, J., Thompson, L., Gordon, S., Newsom, H., Ollila, A., Williams, J., Bentz, J., Nealson, K., Popa, R., Kah, L.C., Moersch, J., Tate, C., Day, M., Kocurek, G., Hallet, B., Sletten, R., Francis, R., McCullough, E., Cloutis, E., ten Kate, I.L., Fraeman, A., Scholes, D., Slavney, S., Stein, T., Ward, J., Berger, J., Moores, J.E., 2014. In situ radiometric and exposure age dating of the Martian surface. Science 343, 1247166. https://doi.org/10.1126/science.1247166.

Fritz, J., Greshake, A., Stöffler, D., 2005. Micro-Raman spectroscopy of plagioclase and maskelynite in Martian meteorites: evidence of progressive shock metamorphism. Antarct. Meteor. Res. 18, 96–116.

Fritz, J., Greshake, A., Fernandez, V.A., 2017. Revisiting the shock classification of meteorites. Meteorit. Planet. Sci. 52, 1216–1232.

Gaffney, A.M., Borg, L.E., Asmerom, Y., Shearer, C.K., Burger, P.V., 2011. Disturbance of isotope systematics during experimental shock and thermal metamorphism of a lunar basalt with implications for Martian meteorite chronology. Meteorit. Planet. Sci. 46, 35–52. https://doi.org/10.1111/j.1945-5100.2010.01137.x.

Hodych, J.P., Dunning, G.R., 1992. Did the Manicouagan impact trigger end-of-Triassic mass extinction? Geology 20, 51–54.

Jaret, S.J., Woerner, W.R., Phillips, B.L., Ehm, L., Nekvasil, H., Wright, S.P., Glotch, T.D., 2015. Makselynite formation via solid-state transformation: evidence of infrared and X-ray anisotropy. J. Geophys. Res., E Planets 120, 570–587. https://doi.org/10.1002/2014JE004764.

Jaret, S.J., Johnson, J.R., Sims, M., DiFrancesco, N., Glotch, T.D., 2018. Microspectroscopic and petrographic comparison of experimentally shocked albite, andesine and bytownite. J. Geophys. Res. 123 (7), 1701–1722.

Jourdan, F., Moynier, F., Koeberl, C., Eroglu, S., 2011. $^{40}Ar/^{39}Ar$ age of the Lonar Crater and consequences for the geochronology of planetary impacts. Geology 39, 671–674.

Jourdan, F., Benedix, G., Eroglu, E., Bland, P., Bouvier, A., 2014. $^{40}Ar/^{39}Ar$ impact ages and time–temperature argon diffusion history of the Bunburra Rockhole anomalous basaltic achondrite. Geochim. Cosmochim. Acta 140, 391–409.

Korochantseva, E.V., Trieloff, M., Buikin, A.I., Hopp, J., 2009. Shergottites Dhofar 019, SaU 005, Shergotty, and Zagami: ^{40}Ar–^{39}Ar chronology and trapped Martian atmospheric and interior argon. Meteorit. Planet. Sci. 44, 293–321. https://doi.org/10.1111/j.1945-5100.2009.tb00735.x.

Korochantseva, E.V., Schwenzer, S.P., Buikin, A.I., Hopp, J., Ott, U., Trieloff, M., 2011. ^{40}Ar–^{39}Ar and cosmic-ray exposure ages of nakhlites — Nakhla, Lafayette, Governador Valadares — and Chassigny. Meteorit. Planet. Sci. 1417, 1397–1417. https://doi.org/10.1111/j.1945-5100.2011.01240.x.

Kuiper, K.F., Deino, A., Hilgen, F.J., Krijgsman, W., Renne, P.R., Wijbrans, J.R., 2008. Synchronizing rock clocks of Earth history. Science 80 (320), 500–504. https://doi.org/10.1126/science.1154339.

Lapen, T.J., Righter, M., Brandon, A.D., Debaille, V., Beard, B.L., Shafer, J.T., Peslier, A.H., 2010. A younger age for ALH84001 and its geochemical link to shergottite sources in Mars. Science 328, 347–351.

Lindsay, F.N., Delaney, J.S., Turrin, D.D., Herzog, G.F., Park, J., Swisher, C.C., 2016. Ar ages of Martian meteorite NWA 7034. In: Proceedings of the 47th Lunar and Planetary Science Conference. Abstract No. 3013.

Nyquist, L.E., Bogard, D.D., Greshake, A., Stöffler, D., Eugster, O., 2001. Ages and geologic histories of Martian meteorites. Chronol. Evol. Mars 96, 105–164.

O'Connell-Cooper, C.D., Spray, J.G., 2011. Geochemistry of the impact-generated melt sheet at Manicouagan: evidence for fractional crystallization. J. Geophys. Res., Solid Earth 116, B06204. https://doi.org/10.1029/2010JB008084.

Park, J., Bogard, D.D., Nyquist, L.E., Herzog, G.F., 2013. Issues in dating young rocks from another planet: Martian shergottites. Geol. Soc. (Lond.) Spec. Publ. 378, 297–316.

Ramezani, J., Bowring, S.A., Pringle, M.S., Winslow, F.D., Rasbury, E.T., 2005. The Manicouagan impact melt rock: a proposed standard for the intercalibration of U–Pb and $^{40}Ar/^{39}Ar$ isotopic systems. Geochim. Cosmochim. Acta, Suppl. 69, 321.

Renne, P.R., Mundil, R., Balco, G., Min, K., Ludwig, K.R., 2010. Joint determination of ^{40}K decay constants and $^{40}Ar^{*}/^{40}K$ for the Fish Canyon sanidine standard, and improved accuracy for $^{40}Ar/^{39}Ar$ geochronology. Geochim. Cosmochim. Acta 74, 5349–5367.

Rubin, A.E., 2015. Maskelynite in asteroidal, lunar and planetary basaltic meteorites: an indicator of shock pressure during impact ejection from their parent bodies. Icarus 257, 221–229.

Sengupta, D., Bhandari, N., Watanabe, S., 1997. Formation age of Lonar Meteor Crater, India. Rev. Fis. Apl. Instrum. 12, 1–7.

Spray, J.G., Thompson, L.M., Biren, M.B., O'Connell-Cooper, C., 2010. The Manicouagan impact structure as a terrestrial analogue site for lunar and martian planetary science. Planet. Space Sci. 58, 538–551. https://doi.org/10.1016/j.pss.2009.09.010.

Stephan, T., Jessberger, E.K., 1992. Isotope systematics and shock-wave metamorphism: III. K–Ar in experimentally and naturally shocked rocks; the Haughton impact structure, Canada. Geochim. Cosmochim. Acta 56, 1591–1605.

Stöffler, D., 1971. Progressive metamorphism and classification of shocked and brecciated crystalline rocks at impact craters. J. Geophys. Res. 76, 5541–5551.

Stöffler, D., Keil, K., Scott, E.R.D., 1991. Shock metamorphism of ordinary chondrites. Geochim. Cosmochim. Acta 55, 3845–3876.

Thomson, S.D., Dickin, A.P., Spray, J.G., 2011. Nd isotope mapping of Grenvillian crustal terranes in the vicinity of the Manicouagan Impact Structure. Precambrian Res. 191, 184–193. https://doi.org/10.1016/j.precamres.2011.08.006.

Tschermak, G., 1872. Die Meteoriten von Shergotty und Gopalpur. Sitzungsber. Math.-Naturwiss. Cl. Kais. Akad. Wiss., Wien 65, 122–146.

Turrin, B.D., Setera, J.B., Park, J., Delaney, J.S., Swisher, C.C., Herzog, G.H., Irving, A.J., 2018. $^{40}Ar/^{39}Ar$ ages of plagioclase-bearing shergottite NWA 4480. In: Proceedings of the 49th Lunar and Planetary Science Conference. Abstract No. 2814.

Van Soest, M.C., Hodges, K.V., Wartho, J.A., Biren, M.B., Monteleone, B.D., Ramezani, J., Spray, J.G., Thompson, L.M., 2011. (U–Th)/He dating of terrestrial impact structures: the Manicouagan example. Geochem. Geophys. Geosyst. 12, 1–8. https://doi.org/10.1029/2010GC003465.

Walton, E.L., Kelley, S.P., Spray, J.G., 2007. Shock implantation of Martian atmospheric argon in four basaltic shergottites: a laser probe $^{40}Ar/^{39}Ar$ investigation. Geochim. Cosmochim. Acta 71, 497–520. https://doi.org/10.1016/j.gca.2006.09.004.

Walton, E.L., Kelley, S., Herd, C.D.K., Irving, A.J., 2014. A laser probe $^{40}Ar/^{39}Ar$ investigation of poikilitic shergottite NWA 4797: implications for the timing of shock metamorphism. Geol. Soc. (Lond.) Spec. Publ. 378, 317–332. https://doi.org/10.1144/SP378.11.

Weirich, J.R., Swindle, T.D., Isachsen, C.E., 2012. ^{40}Ar–^{39}Ar age of Northwest Africa 091: more evidence for a link between L chondrites and fossil meteorites. Meteorit. Planet. Sci. 1335, 1324–1335. https://doi.org/10.1111/j.1945-5100.2012.01397.x.

Wolfe, S.H., 1971. Potassium–argon ages of the Manicouagan–Mushalagan lakes structure. J. Geophys. Res. 76, 5424–5436.

Wright, S.P., Christensen, P.R., Sharp, T.G., 2011. Laboratory thermal emission spectroscopy of shocked basalt from Lonar Crater, India, and implications for Mars orbital and sample data. J. Geophys. Res. 116, E09006. https://doi.org/10.1029/2010JE003785.

Young, K., 2014. The Use of Terrestrial Analogs in Preparing for Planetary Surface Exploration: Sampling and Radioisotopic Dating of Impactites and Deployment of In Situ Analytical Technologies. Arizona State University.